Respiratory Physiology & Neurobiology 265 (2019) 127–140

Contents lists available at ScienceDirect

Respiratory Physiology & Neurobiology

journal homepage: www.elsevier.com/locate/resphysiol

Inputs to medullary respiratory neurons from a pontine subregion that controls breathing frequency

Edward J. Zuperku[a,b,*], Astrid G. Stucke[a,b,c], John G. Krolikowski[a,b], Jack Tomlinson[a,b], Francis A. Hopp[a], Eckehard A. Stuth[a,b,c]

[a] Clement J. Zablocki Department of Veterans Affairs Medical Center, Milwaukee, WI, United States
[b] Department of Anesthesiology, Medical College of Wisconsin, Milwaukee, WI, United States
[c] Pediatric Anesthesia, Children's Hospital of Wisconsin, Milwaukee, WI, United States

ARTICLE INFO

Keywords:
Breathing frequency control
Pons
preBötzinger/Bötzinger complex
Synaptic input
Pre-I neurons
Inspiratory on-switch

ABSTRACT

Neurons in a subregion of the medial parabrachial (PB) complex control expiratory duration (TE) and the inspiratory *on*-switch. To better understanding the underlying mechanisms, this study aimed to determine the types of medullary neurons in the rhythmogenic preBötzinger/Bötzinger Complex (preBötC/BötC) and adjacent areas that receive synaptic inputs from the PB subregion and whether these inputs are excitatory or inhibitory in nature. Highly localized electrical stimuli in the PB subregion combined with multi-electrode recordings from respiratory neurons and phrenic nerve activities were used to generate stimulus-to-spike event histograms to detect correlations in decerebrate, vagotomized dogs during isocapnic hyperoxia. Short-time scale correlations were found in 237/442 or ~54% of the ventral respiratory column (VRC) neurons. Inhibition of E-neurons was ~2.5X greater than for I-neurons, while Pre-I and I-neurons were excited. These findings indicate that the control of TE and the inspiratory on-switch by the PB subregion are mediated by a marked inhibition of BötC E-neurons combined with an excitation of I-neurons, especially pre-I neurons.

1. Introduction

The role of the dorsolateral rostral pons in the control of breathing remains unclear. However, neurons with respiratory related discharge patterns in the parabrachial (PB) and Kölliker-Fuse (KF) regions are referred to as the pontine respiratory group (PRG) and are considered to be mediators of the control and modulation of the breathing pattern. A eupneic breathing pattern, characterized by quiet, regular breaths, requires the entire pontine and medullary portions of the brainstem to be functional and coordinated (St-John and Paton, 2003). With ablation of neurons in a region of the pontine tegmentum, termed the pneumotaxic center, the pattern of respiratory activity is altered to apneusis, which is readily distinguishable from the ramp-like, eupneic inspiratory burst pattern by a more sustained inspiratory duration with a plateau-like pattern, reducing the breathing frequency (fB) (Euler, 1986). As progressively more of the pons is removed, the inspiratory (I) and expiratory (E) phases during apneusis shorten, and with total removal of the pons, the pattern of ventilatory activity is altered to gasping (St-John and Paton, 2003). According to a recent review (Dutschmann and Dick, 2012), the hallmark respiratory function of the PB-KF complex is the regulation of the inspiratory-expiratory (IE) phase transition and the dynamic control of upper airway patency during the respiratory cycle. This assessment may be species dependent (Dutschmann and Dick, 2012). In dogs, where typical apneustic patterns are only occasionally observed, a subregion in the medial PB complex appears to play a key role in the control of expiratory duration (TE), the expiratory-inspiratory (EI) phase transition and hence breathing frequency (Zuperku et al., 2017). Within this subregion, excitation of neurons produces increases in fB, while inhibition or disfacilitation of these neurons produces bradypnea and apnea. In particular mu-opioid inhibition of these neurons leads to marked bradypnea and apnea (Prkic et al., 2012). In addition, the bradypnea induced by systemic administration of mu-opioids at clinical concentrations can be reversed by local microinjections of naloxone within the subregion. Neurons within the canine PB region have both phasic respiratory-modulated patterns and non-respiratory modulated tonic patterns (Zuperku et al., 2015b). Currently, it is not clear whether the induced changes in fB are due to neurons with phasic or tonic discharge patterns or both.

When this subregion was electrically stimulated with a bipolar microelectrode during the E-phase, there was a powerful shortening of TE that was dependent on the stimulus frequency (Zuperku et al., 2017). Short 100–200 ms pulse-trains that were delayed relative to the

* Corresponding author at: Research Service/151, Zablocki VA Medical Center, 5000 W. National Avenue, Milwaukee, WI 53295, United States.
E-mail address: ezuperku@mcw.edu (E.J. Zuperku).

https://doi.org/10.1016/j.resp.2018.06.011
Received 15 February 2018; Received in revised form 10 May 2018; Accepted 4 June 2018
Available online 28 June 2018
1569-9048/ Published by Elsevier B.V.

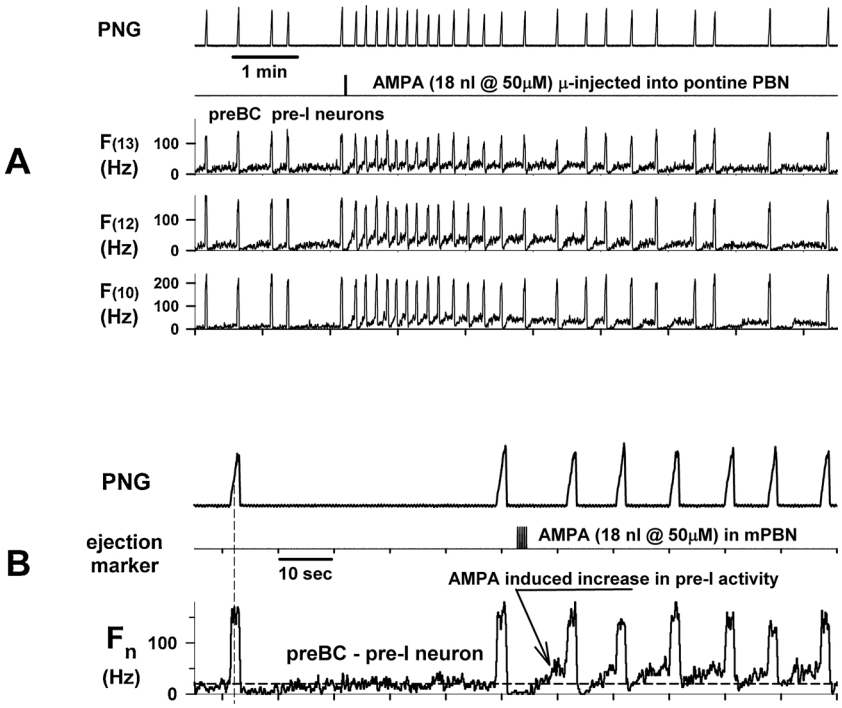

Fig. 1. An increase in the pre-I activity of preBötC pre-I neurons induced by microinjection of AMPA into the pontine PB subregion is associated with tachypnea. A) Responses of the phrenic neurogram (PNG) and the discharge frequency patterns (F from probe electrodes 10,12, and 13) of 3 pre-I neurons in the preBötC region to microinjection of 18 nl of AMPA into the PB subregion. Note the increase in the pre-I activity immediately after the AMPA microinjection. B) Data shown on an expanded time scale show the activity from the pre-I neuron recorded on electrode 12. Dashed horizontal line shows pre injection baseline activity.

beginning of the E-phase were capable of evoking a "eupneic" phrenic burst pattern and that was no different than the spontaneous burst pattern indicating that the I-phase generating network contains pacemaker-like neurons with self-regenerating properties capable of producing a stereotypic ramp-like phrenic burst pattern. The contour and duration of this burst pattern, when triggered at various delays > 1 s is unchanged, suggesting that the control mediated by this pontine subregion is purely one of phase-timing, that is the shortening of TE and initiation of the I-phase.

In an attempt to better understand the underlying mechanisms, we inserted a 16-electrode probe into the preBötzinger Complex (preBötC) region of dogs and a glass micropipette into the pontine subregion to induce increases in fB by microinjecting AMPA. An example showing the response of several pre-I/I-constant neurons to AMPA is shown in Fig. 1. Microinjection of AMPA (18 nl) produced tachypnea, which was preceded by increases in the pre-I activity of several pre-I neurons, which are considered putative pacemaker neurons, suggesting a possible mechanism producing tachypnea. The ramp pattern of the phrenic neurogram (PNG) was preserved and changes were mainly in TE and not inspiratory duration (TI).

The aim of the current study was to determine in more detail the types of medullary neurons in the preBötC /Bötzinger Complex (BötC) and adjacent areas that receive synaptic inputs from the pontine subregion and explore if these inputs are excitatory or inhibitory in nature. Because of the relatively slow dynamics associated with AMPA-induced excitation due to diffusion and receptor binding properties, we focused on electrical stimulation via a concentric bipolar microelectrode to rapidly activate the subregion neurons at 10 Hz. The changes in the probability of neuronal firing were analyzed using stimulus-to-spike correlation histograms also referred to as post-stimulus time-histograms (PSTHs). Significant deviations in the PSTH from baseline discharge rates were used as evidence for the existence of a synaptic input, which could be either excitatory or inhibitory. The findings of this study indicate that the control of TE and the inspiratory on-switch by the pontine subregion in the medial PB complex is mediated by the combined action of a marked inhibition of BötC E-neurons and excitation of I neurons, especially pre-I neurons.

2. Materials and methods

2.1. Animals

This research was approved by the subcommittee on animal studies of the Zablocki Department of Veterans Affairs (VA) Medical Center in accordance with provisions of the Animal Welfare Act, the Guide for the Care and Use of Laboratory Animals, and VA policy. Experiments were performed on 11 Beagle dogs of either sex, weighing 9–12 kg. Inhalational anesthesia was induced by mask and maintained with isoflurane at 1.5–2.5% end-tidal concentration. The animals were monitored for signs of inadequate anesthesia such as salivation, lacrimation, and increases in blood pressure and heart rate. If required, anesthetic depth was increased immediately.

2.2. Surgical procedures

The anesthetized dogs were intubated with a cuffed endotracheal tube and their lungs mechanically ventilated with an air-O2-isoflurane mixture. A femoral artery was cannulated for blood pressure recording and a femoral vein for continuous infusion of maintenance fluids and administration of drugs. The animals were positioned in a stereotaxic device (model 1530; David Kopf Instruments, Tujunga, CA) with the head ventrally flexed (30°). A bilateral pneumothorax was created with bilateral thoracotomy tubes open to air to minimize brain stem movement and phasic inputs from chest wall mechanoreceptors. The animal was decerebrated by midcollicular transection (Tonkovic-Capin et al., 1998), and then isoflurane anesthesia was discontinued. The animals were ventilated with an air-O2 mixture and maintained in hyperoxic isocapnia (FIO2 > 0.6, end-tidal CO2 range 40–50 mmHg). Complete access of the dorsal surface of the brain stem was obtained by an occipital-parietal craniotomy followed by cerebellectomy and external sagittal and nuchal bone crest removal. After bilateral neck dissections, phrenic nerve activity was recorded from the desheathed right C5 rootlet. Bilateral vagotomy was performed to achieve peripheral deafferentation to avoid interference of the mechanical ventilation with the underlying central respiratory rhythm and respiratory neuronal activity. The PNG was obtained from the moving-time average (time-constant: 100 ms) of the amplified phrenic nerve activity and was used

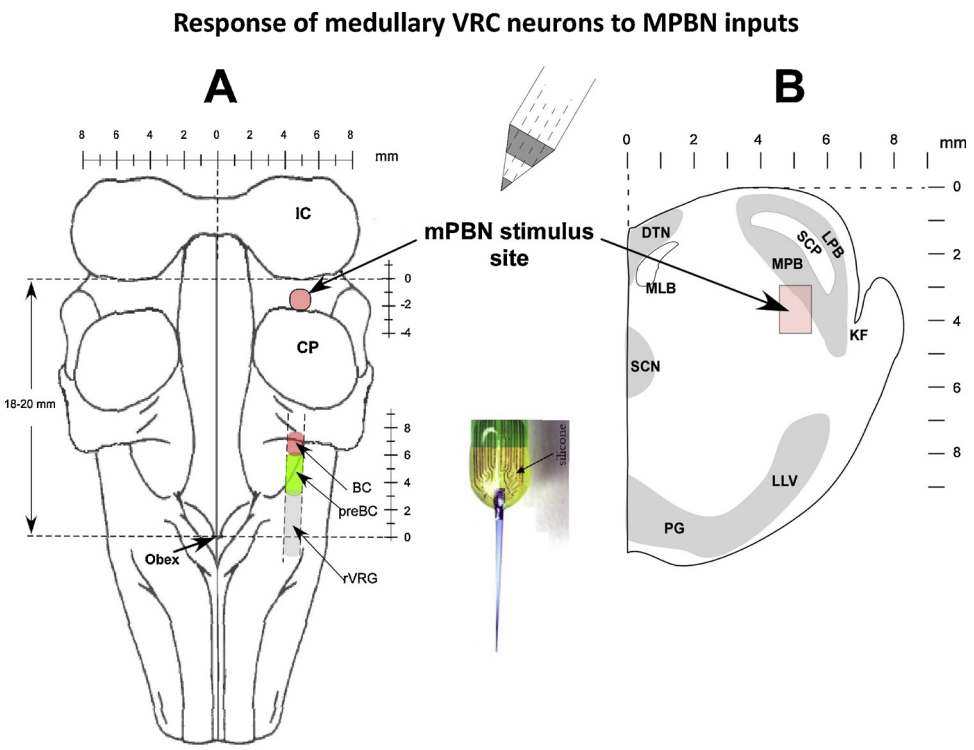

Fig. 2. Diagram illustrating the methods used. A) Dorsal view of the brainstem showing the stimulating and recording sites. Stimuli were applied in the PB subregion via a concentric bipolar microelectrode and a NeuroNexus 16-electrode probe was used for recording in the medullary ventral respiratory column (VRC). B) Transverse section of rostral pons showing the PB subregion that controls breathing frequency where the stimuli were applied (arrows). mPBN: medial parabrachial nucleus, BC: Bötzinger Complex; preBC: preBötzinger Complex; rVRG: rostral ventral respiratory group; DTN, dorsal tegmental nucleus; KF, Kölliker-Fuse nucleus; LLV, lateral lemniscus ventral nucleus; LPB, lateral parabrachial nucleus; MLB, medial longitudinal bundle; MPB, medial parabrachial nucleus; PG, pontine gray; SCN, superior central nucleus; SCP, superior cerebellar peduncle.

to produce timing pulses corresponding to the beginning and end of the inspiratory phase for the measurement of TI and TE. Peak phrenic activity (PPA) was also obtained from the PNG. Continuous neuromuscular block was achieved with cisatracurium besylate (1 mg/kg bolus, followed by 0.5 mg/kg/h IV infusion) to reduce motion artifacts during neuronal recordings. Esophageal temperature was maintained at 38.5 ± 0.5 °C with a heating pad. Mean arterial pressure was maintained above 80 mmHg with adjustment of intravenous fluids and, when needed, phenylephrine infusion (0.5–5 μg/kg/min).

2.3. Multielectrode recording of ventral respiratory column neuronal activity

Respiratory neuronal activity was recorded from the VRC using a NeuroNexus 16-electrode probe (A1 × 16–10 mm-100–177-A16; www.neuronexus.com). The 16 electrodes were linearly arranged with an inter-electrode spacing of 100-μm. In each dog, multiple sets of recordings were made within the VRC from the rostral Ventral Respiratory Group (rVRG), preBötC, BÖTC, and retrofacial regions (Fig. 2). Probe insertions were spaced 0.5 to 1 mm apart. Stereotaxic coordinates of the probe tip, the location of each of the 16 electrodes and the tilt angle of the medulla for each dog were used to assign a location to each recorded neuron. The probe output connected directly with a dual inline socket equipped with 16 miniature preamplifiers (4x gain; Tucker-Davis model RA16AC4; www.tdt.com). The preamplified signals were further amplified (3000x) and bandpass filtered (0.3–3 kHz; CWE 16-channel System 2000; www.cwe-inc.com). The signals were digitized at 20 kHz/channel with 16-bit resolution with a Cambridge Electronic Design CED 1401 mk II and displayed and analyzed using Spike2 software (ver. 7.16). Stimulus sync pulses, stimulus frequency pattern and phrenic nerve activity were also recorded.

2.4. Electrical stimulation technique

A concentric bipolar electrode was positioned in the medial PB region 4.5–5.5 mm lateral to the pontine midline and 2–3 mm caudal to the caudal pole of the inferior colliculus (IC). This location has previously been shown to produce robust tachypneic responses to (±)-a-Amino-3-hydroxy-5-methylisoxazole-4-propionic acid (AMPA) microinjections. The concentric electrode (FHC #CBCPE75; Bowdoin, ME) consisted of a 50-μm platinum/iridium inner electrode and a 250-μm stainless steel 10 mm long outer electrode, insulated up to the tip, with an epoxy seal between the electrodes. The pencil-point tip with a grind angle of 45 degrees results in an average separation between electrodes of ~175-μm, which was sufficient to locally depolarize enough neurons to obtain robust effects at low current strengths. While small in diameter, this configuration is durable and can be reused multiple times (Fig. 2).

A programmable constant-current stimulator was used to deliver continuous pulses and pulse-trains with step frequency patterns synchronized to the onset of the I- or E-phase. The stimulus strength was adjusted to 1.2–1.4 times the minimum threshold level that induced a decrease in TE, typically 80–120 μA and 100-μs in pulse duration. If necessary, the electrode was repositioned to optimize the tachypneic response. Using step frequencies of 50–100 Hz applied every other phrenic burst cycle, the electrode was slowly lowered from the dorsal surface until a depth was reached at which an optimal response was obtained. By delivering the stimulus every other phrenic burst cycle, it was easy to compare the effect of the stimulus on TE versus the adjacent no-stimulus control cycles.

2.5. Microinjection technique

Multibarrel micropipettes (10–30 μm composite tip diameter) consisting of a recording barrel containing a 7-μm-thick carbon filament and three drug barrels were used for pressure microinjections. Recordings of respiratory-related neuronal activity within the medial PB region were used as a guide, especially for depth from the dorsal pontine surface, to locate the tachypneic region via AMPA microinjections. Adjustments in the lateral (midline) and caudal (inferior colliculus) coordinates were used to determine the most sensitive response location. Microinjections consisted of the glutamatergic agonist AMPA (15–50 μM; at 18–76 nl), which was dissolved in artificial cerebrospinal fluid (ACSF). AMPA was placed in more than one barrel to have a

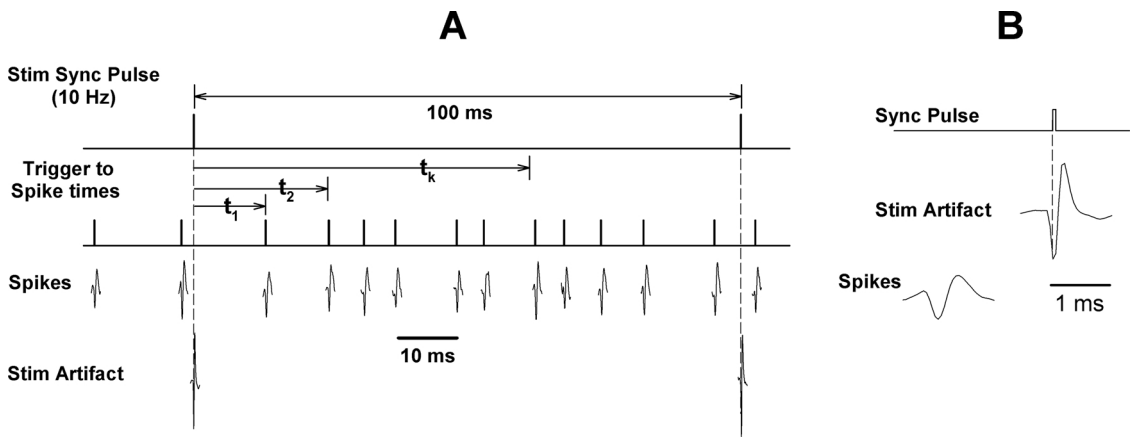

Fig. 3. Illustrates the method for processing data to generate stimulus-to-spike correlation histograms or post-stimulus time histograms (PSTHs). A) Stimulus sync pulses serve as the time reference. A stimulus rate of 10 Hz provides an inter-stimulus interval of 100-ms. A standard pulse shown above each spike is used to obtain the times of spike occurrences relative to the stimulus sync pulse: t_1, t_2,….t_k. B) The PB subregion stimuli produced stimulus artifacts (seen below the sync pulse) in the neuronal recordings, but they were typically higher and narrower than the spikes and were removed using the Spike2 sorting software.

backup if a barrel became obstructed. The microinjected volumes were measured via height changes of the meniscus in the pipette barrel with a 100x magnification microscope equipped with a reticule (resolution: ~2 nl).

Arterial blood pressure, airway CO_2 concentration, microinjection marker, stimulus frequency pattern, breath-to-breath TI, TE, and PNG signals were continuously recorded online with a PowerLab system (ADInstruments, Castle Hill, Australia; 16SP and LabChart). Post experiment LabChart data was exported to SigmaPlot 11 (Systat Software, San Jose, CA) for data reduction, data plotting and statistical analysis. Software algorithms, written in SigmaPlot transform language were used to calculate cycle-to-cycle values of TI, TE, peak PNG (PPA), and stimulus frequency, and imported Spike2 neuronal rate-meter patterns, cycle-triggered histograms (CTH) of neuronal data and stimulus-spike event correlations.

For the analysis for synaptic connections, the pontine stimulus frequency was set at 10 Hz for 10 min. This provided ~6000 stimulus triggers with an inter-stimulus interval of 100-ms (Fig. 3). The intervals from the sync pulse to each spike (t_k; Fig. 3) were use to create a stimulus-to-spike interval histogram (Event Correlation; Spike2)

2.6. Analysis of stimulus-to-spike histograms

Post stimulus time-histograms (PSTHs) provide a means to observe changes in the probability of firing following the stimulus. Deviations from the mean baseline frequency indicate that the stimulus altered the activity in the recorded neuron, either via excitation and/or inhibition. An example of our analysis obtained from a BötC E-neuron is shown in Fig. 4. The PSTH was generated in Spike2 as an Event Correlation with a duration of 100-ms, using a bin width of 0.2-ms and a 2-ms pre stimulus offset. The last 40–50 ms of the PSTH was used to calculate the mean and SD of the activity during relative quiescence, which would correspond to the level that would be measured with a stimulus current of zero. Threshold levels of ± 2 SDs were used (dashed horizontal lines). In addition the PSTH was smoothed using a 5-point running average (red line; Fig. 4). The time regions, where the PSTH (red) exceeded either the two thresholds, are indicated by the thick black lines superimposed on the mean level. Using this information for significant deviations, the latency, duration, the average discharge frequency during the deviation (vertical arrow) and the area of the deviation (aveF x duration; shaded region only illustrated for the first deviation, Fig. 4) were calculated. This PSTH indicated 5 significant deviations. The earliest and largest negative deviation suggests that this neuron received a strong inhibitory synaptic input from the pontine subregion. The large, short duration dip at the beginning of the PSTH is due to the presence of the stimulus artifact.

2.7. Histology

At the conclusion of several experimental protocols, bilateral microinjections (0.5–1 µl) of fluorescent latex microspheres (Lumafluor.com; Red Retrobeads), diluted to 5% of the supplied concentration, were used to mark the stimulation sites for histological analysis. The brain stems were removed postmortem and submersed in paraformaldehyde fixative (4%) for 1 wk before being frozen and sectioned. Sequential sections (of 25 µm thickness) were cut from 2-mm rostral to 5 mm caudal to the caudal edge of the IC. Alternate sections were stained with neutral red for histological identification of nuclear groups and compared with unstained adjacent sections showing fluorescent beads.

2.8. Statistical analyses

The latency, duration, average F and area data, derived from the PSTH analysis, were grouped into 7 categories corresponding to discharge patterns of 7 types of medullary respiratory neurons: pre-I, I, I-dec, I-aug, E, E-dec and E-aug. A one-way ANOVA was used to analyze differences among the neuron subtypes for the variables previously mentioned. A two-way ANOVA was used to test for differences in anatomic location (rostral-caudal and depth from dorsal surface) among neuron subtypes that received a synaptic input and those that did not. The Holm-Sidak method was used for pair wise multiple comparisons with a family-wide error rate of 0.05. For all data sets, tests for normality (Kolmogorov-Smirnov test) were performed before parametric procedures were used. For data sets that failed the normality test a Kruskal-Wallis one-way ANOVA on ranks was used with Dunn's method for multiple comparisons versus control group. Differences were considered significant at $P < 0.05$. Values are expressed as means ± SE.

3. Results

3.1. Synaptic connections revealed by PSTH analyses

An association of significant deviations in the PSTHs secondary to the effect of pontine inputs on the spontaneous neuronal discharge patterns is clearly discernable. For example, the data for the PSTH shown in Fig. 2, which showed an early large negative deviation, was taken from the BötC E-neuron shown in Fig. 5. There is a marked reduction in discharge frequency, Fn, during the 25 Hz stimulus, as well

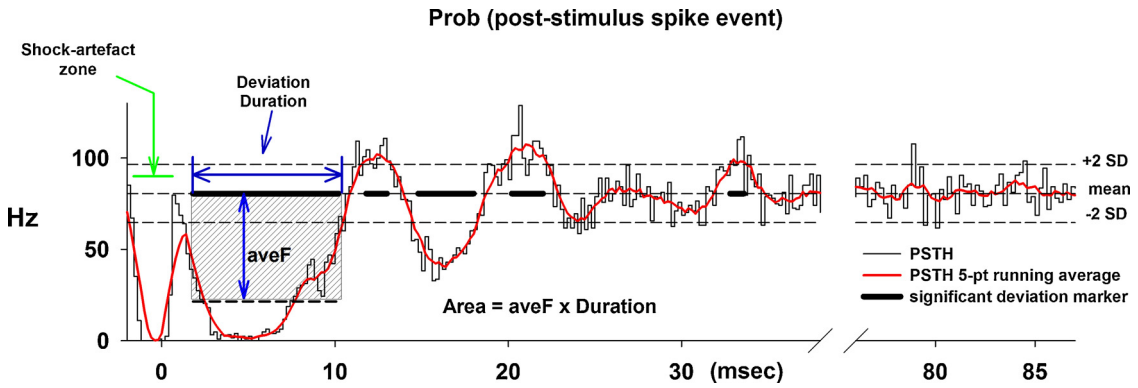

Fig. 4. An example of a post-stimulus time histogram (PSTH) obtained from an E-neuron in the Bötzinger region shows the method of analysis used to determine the presence of synaptic inputs to the recorded neuron from the PB subregion stimulus. The average post-stimulus discharge frequency is calculated as number of (spikes/bin)/(bin-width)/(number of trigger events). A change in the probability of the neuron discharging due to the stimulus is shown by a deviation in the histogram from a baseline level. This baseline level typically occurs during the last 50-ms of the histogram when the neuronal activity is unperturbed by the stimulus. The average discharge frequency and standard deviation were calculated during the last ~50 ms of the PSTH (right) and used to set reference levels for the mean ± 2 SDs shown as dash horizontal lines. A 5-point running average was used to smooth the data (red line). The times of significant deviations were marked (thick black line segments superimposed on the baseline level). For each of these marked regions, the latency, duration, average frequency during the deviation relative to baseline and the area of the deviation were calculated (shaded region). The first few ms of the PSTH shows the shock-artifact zone that results from sorting out the stimulus artifact from the neuronal recording.

as a marked decrease in TE. At step frequencies > 50 Hz, the neuron discharge was completely inhibited (silenced) during the stimulus (data not shown). The associated PSTH (Fig. 4) suggests that the inhibition was due to a volley of inhibitory post-synaptic potentials (IPSPs) with very short latencies (2–5 ms). With a conduction distance between stimulus and recording sites of ~10 mm, the estimated conduction velocity would be 2–5 m/s.

In another example of data from a pre-I neuron, the PSTH showed a marked and significant increase in the probability of firing suggesting an excitatory synaptic input from the pontine subegion (Fig. 6). The cycle-triggered histogram (CTH) shows the ramp-like increase in neuronal activity during the E-phase. As suggested via modeling studies of pacemaker neurons (Butera et al., 1999), the increase in pre-I activity has been proposed to be responsible for triggering the I-burst. The auto-correlogram shows no activity at and near zero time, suggesting the spike data was from a single neuron. The ongoing spontaneous activity of the pre-I neuron for cycles with a longer duration pulse-train showed a stimulus-induced increase in pre-I activity that can be seen in both the rate-meter output and in the spike activity (Fig. 7). The more delayed pulse train (8 s) had a much shorter duration due to onset of the I-phase.

Examples of PSTHs for the 7 types of respiratory neurons with corresponding CTHs of their discharge profile and auto-correlograms are shown in Fig. 8 for I-aug, I-dec and I neurons (left panel) and in Fig. 8 (right panel) for an E-aug and an E-dec neuron. The I-aug neuron showed an early small negative deviation (Fig. 8, A2) suggesting the presence of a small inhibitory input in this example. The PSTH of the I-dec neuron (Fig. 8, B1 and B2) showed an early strong inhibition followed by a much later excitation. The PSTH of the I-neuron (Fig. 8, C1 and C2) also showed an early long lasting inhibition along with a strong superimposed excitatory input centered at ~ 8-ms, indicating that this medullary neuron received inputs from different fibers that were simultaneously activated in the pontine subregion but with different conduction velocities. In the E-aug neuron example (Fig. 8, right panel, A1 and A2), the PSTH showed an early small positive deviation immediately followed by a small negative deviation suggesting a weak excitatory input followed possibly by a refractory period. The PSTH of the E-dec neuron (Fig. 8B1 and B2) showed 3–4 short periods with small but significant negative deviations, suggesting inhibitory inputs from neurons with different conduction velocities.

3.2. Group data for synaptic connection analysis

Approximately 54% of 442 neurons in 11 dogs had significant deviations in their PSTHs consistent with excitatory and/or inhibitory pontine inputs. For the group data in Fig. 9, the data of only the largest positive and/or negative deviations for each neuron PSTH were used,

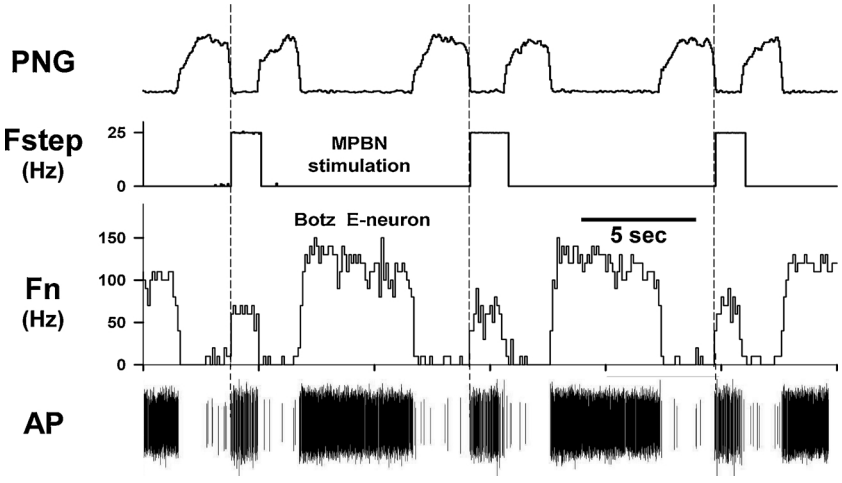

Fig. 5. Recordings from an E-neuron in the Bötzinger region showing the effects of PB subregion stimulation with 25 Hz step stimulus patterns delivered every other cycle during the E-phase. Data from the same neuron analyzed in Fig. 4 that shows a large significant negative deviation shortly after the stimulus indicating a reduction in the probability of firing due to an inhibitory input. Note the powerful reduction in discharge frequency (Fn) along with the shortening of TE. Higher stimulus frequencies (not shown) silenced the neuron. Fstep: stimulus frequency; AP: action potentials.

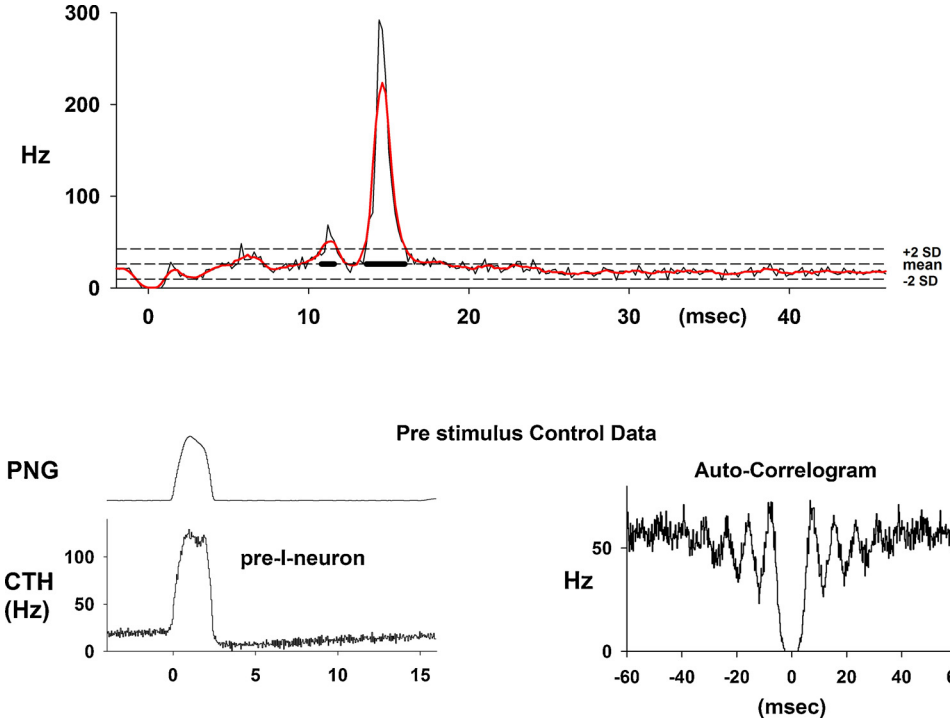

Fig. 6. Upper: An example of a PSTH of the activity from a pre-I neuron that shows a very marked increase in the probability of firing with a latency of ~13-ms. The respiratory cycle-triggered histogram (lower left) shows a ramp increase in activity during the E-phase before the I burst activity. The auto-correlogram indicates that the data represent the activity of a single neuron, since there is no activity close to the zero time from other neurons.

based on the area parameter. The neurons were sorted according to their discharge patterns into 7 categories. These data are shown by the box plots of Fig. 9A and B. Differences among the neuron subtypes were analyzed with a one-way ANOVA on ranks (Kruskal-Wallis; $p < 0.05$). There was a significant difference between magnitude of the negative deviation of the Area variable of the E-neurons and pre-I and I-aug neurons (Fig. 9A; a and b), but no differences among neuron subtypes for the positive deviations. For the ave-F variable, there were no differences among neuron subtypes for both the (+) and (−) deviations (Fig. 9A, lower). There were some differences in the latencies among neuron subtypes (Fig. 9B), where it appears that the latencies of the I-neurons are shorter. Differences among neuron subtypes for the deviation duration (Fig. 9B) are correlated with those of the Area variable. A longer duration would result in a larger area (area = ave-F x Duration), especially since there were no differences in ave-F among the neurons.

When all subtypes of I-neurons and all subtypes of E-neurons are pooled together, some more general observations can be made (Fig. 10A). The latencies of the I-neurons are typically shorter, especially for the (+) deviations, which are related to excitatory inputs. The duration of the (−) deviations, associated with inhibitory inputs, for the E-neurons was clearly longer lasting than for the I-neurons (Fig. 10A). There was no difference in the magnitude of the deviations (ave-F, Fig. 10A) between the I- and E-neurons. The Areas of the (−) deviations for the E-neurons were significantly greater that those for the I-neurons (Fig. 10A, bottom), but no differences were observed for the Areas of the (+) deviations for the two-neuron types. This suggests that the E-neurons are receiving a much larger amount of inhibition mediated by the pontine neurons. Fig. 10B shows the ratio of the number of neurons having an excitatory input to those having an inhibitory input for each neuron subtype. For example, three times more pre-I neurons received an excitatory input than an inhibitory input. Also the I-neurons received more excitatory inputs than inhibitory inputs compared with the E-neurons. This suggests that the I-neurons are more likely to receive an excitatory input than an inhibitory input from the pontine subregion, while the E-neurons are just as likely to receive either type of

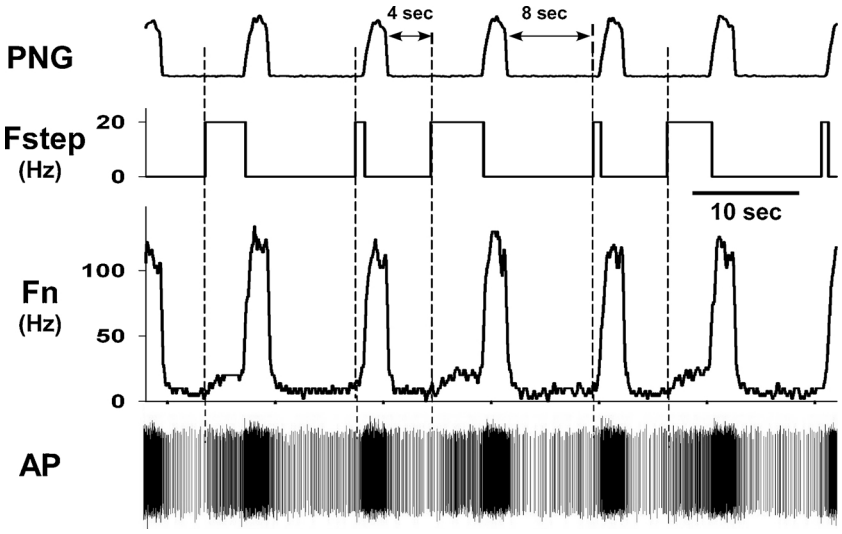

Fig. 7. Data from the pre-I neuron shown in Fig. 6 shows how a delayed stimulus train during the E-phase increases neuronal activity. The pulse-train with a 4-sec delay, which was delivered every other cycle, produced an increase in the discharge frequency (Fn and spike density) just before the onset of the I-phase. The duration of pulse-trains with the 8-sec delay were shortened by the onset of the I-phase and thus too short to have much of an effect.

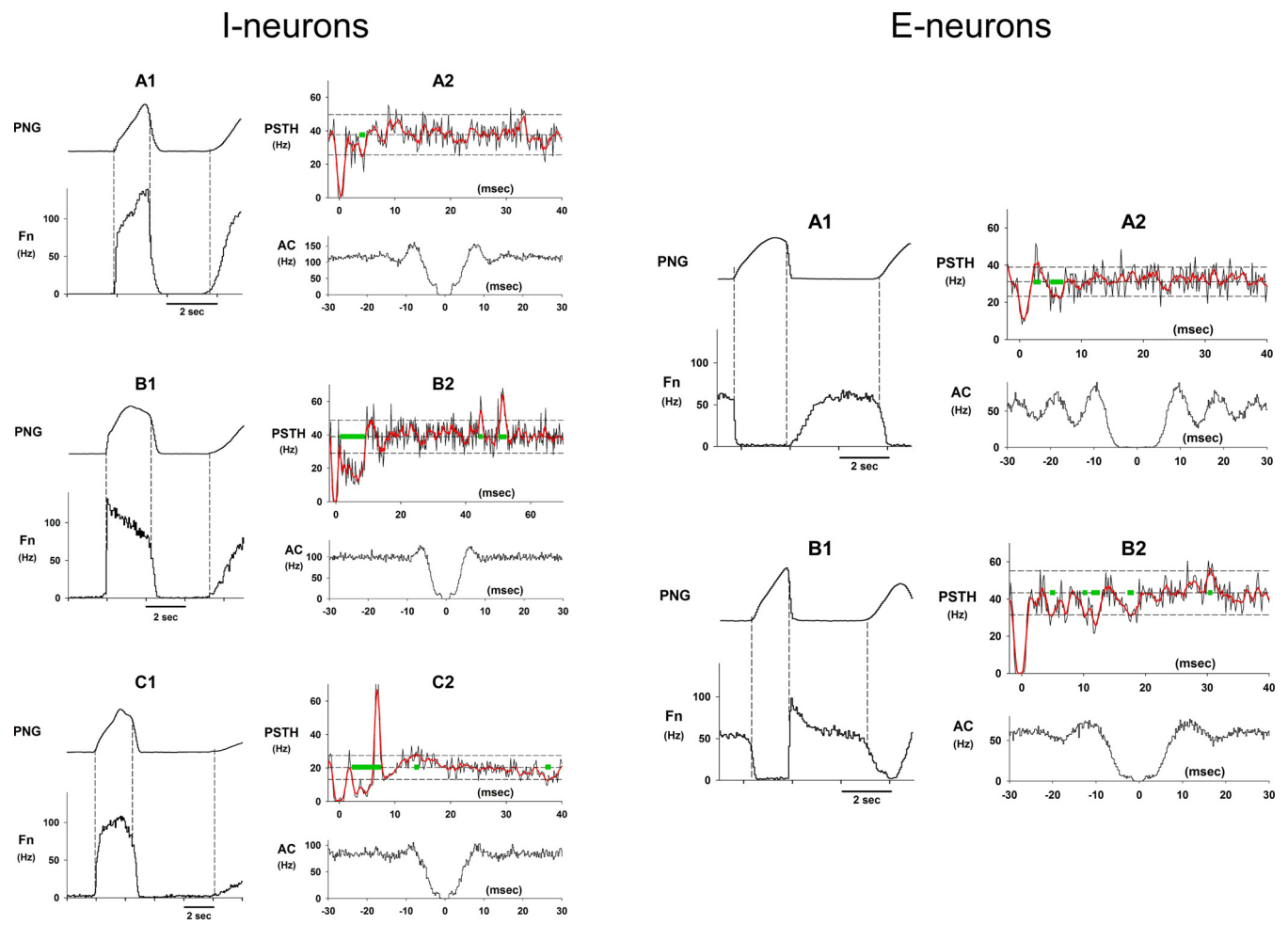

Fig. 8. Examples of the discharge patterns, PSTHs and auto-correlograms for various subtypes of I-neurons and E-neurons within the VRC of the medulla. The green bars along the mean baseline frequency level indicate the times and durations of the significant deviations. The PSTH (A2) of the I-aug neuron (A1) shows an early short negative deviation indicative of an inhibitory input. The PSTH (B2) of the I-dec neuron (B1) shows an early marked significant deviation indicative of relatively strong inhibitory inputs. Also seen was a delayed (~50-ms) positive deviation suggesting an excitatory input. The PSTH (C2) of an I-neuron (C1) shows a complex deviation pattern. It suggests an early marked long-lasting period of inhibition with a marked positive deviation superimposed, possibly from an excitatory input. The PSTH (A2) of an E-neuron with an augmenting-like pattern (A1) shows small early positive deviation followed by a small negative deviation indicative of weak synaptic inputs. The PSTH (B2) of an E-dec neuron (B1) shows what appears to be a number of relatively weak inhibitory inputs with different conduction delays.

input. However as already stated, the E-neurons appear to be more strongly inhibited.

3.3. Anatomical location of neurons receiving inputs from the pontine subregion

Stereotaxic coordinates relative to the obex, midline and dorsal surface were use to plot the locations of the seven subtypes of neurons that had PSTHs with significant deviations. The coordinates were corrected for the tilt angle of the medulla for each dog, where a positive value indicated a downward tilt of the nose. The 5th, 25th, 50th, 75th and 95th percentiles were 2.8, 8.9, 13.3, 14.7, and 19.0 degrees, respectively. The plots show the depth from the dorsal surface and the distance rostral to the obex. Since the VRC in the dog is narrow and consistently located at ~ 4.5 mm lateral to the midline, the plots used data from all the neurons regardless of the midline coordinate. The relationship between the pre-I neurons and the BötC E neurons is shown in the upper plot of Fig. 11. While there is some overlap, there is a distinct separation between the two groups, where the pre-I neurons were more caudal (median values 4.6 vs. 6.2 mm, $p < 0.001$, Mann-Whitney Rank Sum Test) and somewhat more dorsal to the E-neurons (mean 6.5 ± 0.13 vs. 7.0 ± 0.1; $p < 0.001$; *t*-test). These data are consistent with the currently held view of the preBötC being caudal to the BötC although there is clearly considerable overlap. The I-dec neurons were in general slightly more caudal (median: 5.9 vs. 7.0, $p = 0.016$) and dorsal (mean: 6.7 ± 0.16 vs. 7.3 ± 0.18, $p = 0.017$, t-test) to the E-dec neurons (middle plot, Fig. 11). The I- and I-aug neurons were distributed from the rostral VRG to VRC locations rostral to the BötC (bottom plot, Fig. 11). The I-aug neurons were in general slightly more dorsal to the I-neurons (median: 6.8 vs. 7.3, $p = 0.025$, Rank Sum test), but overlapped in the caudal-rostral direction.

3.4. Anatomical locations of neurons with versus without pontine inputs

Plots of the depth from the dorsal surface and the distance rostral to the obex for the various subtypes of neurons with (red) and without (blue) pontine subregion inputs are shown in Fig. 12A. The percentage of neurons in each subtype that received an input from the pontine subregion is as follows: 73.7% pre-I, 65.7% E & Eaug, 46.9% Edec, 52.9% Idec, 49.5% Iaug, and 43.1% I. Mere visual inspection suggests that there is considerable overlap in location. However, a two-way ANOVA with factors of neuron subtype and input status suggested that there were some differences in location (Fig. 12B). With respect to the rostral-caudal dimension, the pre-I neurons with a pontine subregion input tended to be located more rostral to the pre-I neurons without inputs (Fig. 12B, left, A–P). With respect to the depth from dorsal

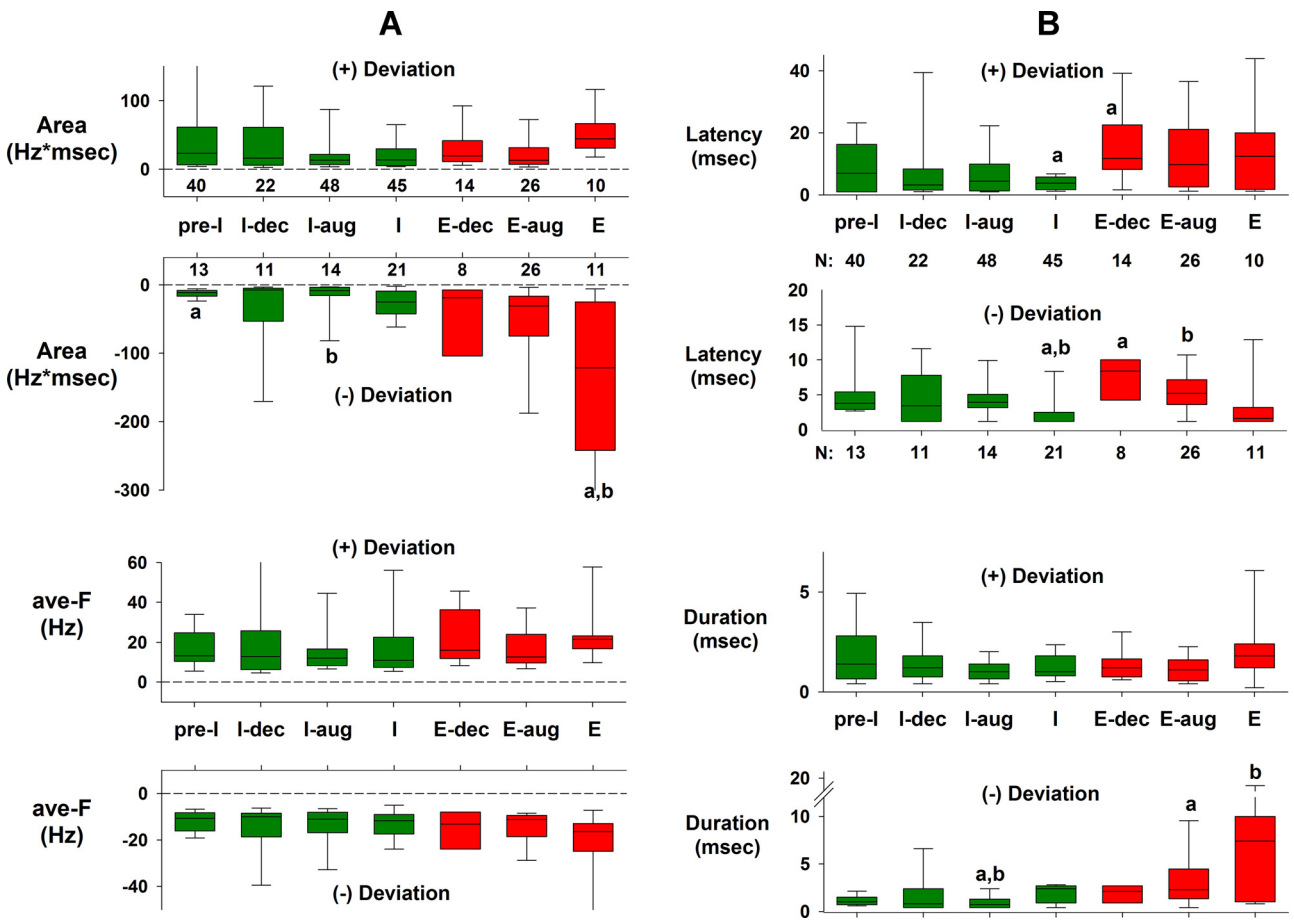

Fig. 9. Group data for the largest significant positive (+) and/or negative (−) deviations for each subtype of medullary neuron. A) Data for the Area parameter (upper) and average deviation frequency (ave-F, lower). The size of the bars reflects the magnitude of the synaptic input. B) Data for the deviation latency (upper) and duration (lower). Green bars: data for I-neurons; red bars data for E-neurons. Numbers below or above the upper bar graphs indicate the number of neurons having positive and negative significant deviations. Significant differences (one-way ANOVA on ranks) between the bars are indicated by lower case a and b symbols. Note that the Areas for the (-) deviations of the E-neurons are clearly larger than those for the I-neurons, mainly due to the larger durations (B, bottom), while ave-F was not different among the groups. See text for details.

surface dimension (Fig. 12B, right), comparison of pre-I neurons suggested that those with a pontine subregion input tended to be located more ventral to those without an input. For I-aug neurons, those receiving an input were more ventral than those without an input. For E- and Eaug neurons, those receiving an input were more dorsal to those without an input. (Fig. 12A upper-right plot).

4. Discussion

Unit recordings from VRC respiratory neurons during electrical stimulation of the pontine subregion in conjunction with post-stimulus event-correlation analysis were used to determine whether various neuron subtypes received synaptic input from the pontine subregion that controls the phrenic burst rate. Analysis of the PSTHs showed positive and/or negative significant deviations in the probability of firing in 237 of 442 neurons suggesting that ~53.6% of the recorded neurons received a synaptic input from the pontine subregion. The magnitude of significant changes in the probability of a neuron firing following a pontine stimulus pulse was quantified by measurement of the average amplitude of a deviation and its duration (e.g. Fig. 4). The product of these two parameters was calculated as the area of the neuronal response curve (Area = aveF x duration) relative to the quiescent baseline activity and used to consolidate these two parameters into one that estimated the effective size of the synaptic input. Since the PSTHs of many of the neurons had more than one significant deviation, only the largest positive and/or negative deviations based on the response area parameter were used in order to simplify the analysis of the group data. These data are summarized in Figs. 9 and 10 for 7 subtypes of VRC neurons. A key finding was that the E-neurons are much more strongly inhibited than the I-neurons (Fig. 10A, Area), while the I-neurons were much more likely to be excited than the E-neurons (Fig. 10B).

4.1. Pre-I neurons

The pre-I neurons, also referred to as I-driver (Segers et al., 1987) (Lindsey et al., 1987) and considered to have pacemaker properties (Schwarzacher et al., 1995), were primarily excited by the pontine input with very little inhibition (Fig. 9A, Area). They appear to be located in the region of the preBötC (Fig. 11, top plot, green shaded region), which is functionally identified in the dog via tachypneic responses to glutamate agonist microinjections in the VRC (Jakovcevic et al., 2005). In addition (as seen in Fig. 1), an increase in the pre-I activity of pre-I neurons was associated with an increase in phrenic burst rate, suggesting that the tachypnea induced by the microinjection of AMPA in the pontine subregion resulted from the increase in the pre-I activity of these preBötC pre-I neurons. An example of this increase in pre-I activity of a pre-I neuron was also seen during electrically-induced activation of the pontine subregion (Fig. 7). The corresponding PSTH shows a large positive deviation at ~15-ms (Fig. 6, top).

These results suggests a possible mechanism whereby an increase in medial PB activity increases the excitation to the preBötC pre-I neurons,

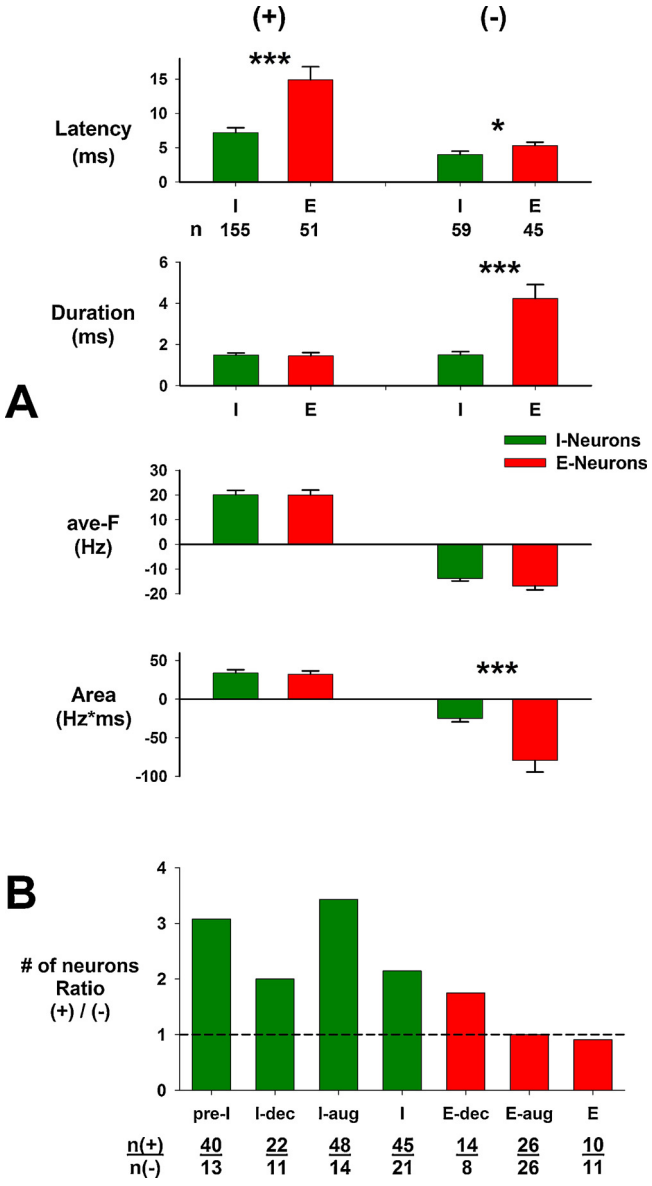

Fig. 10. A) Group data for all I-neurons and E-neurons pooled for (+) and (-) deviations as indicated at top. Significant differences between the I- and E-neurons are indicated by asterisks: * $p \leq 0.05$; *** $p \leq 0.001$. n: number of neurons in groups. See text for details. B) Data for the ratio of number of neurons with (+) deviations to the number of neurons with (-) deviations for the 7 subtypes of neurons shown below bars [n(+)/n(−)]. Green: I-neurons; red: E-neurons. Note that the I-neurons are more likely to have excitatory inputs than the E-neurons. See text for details.

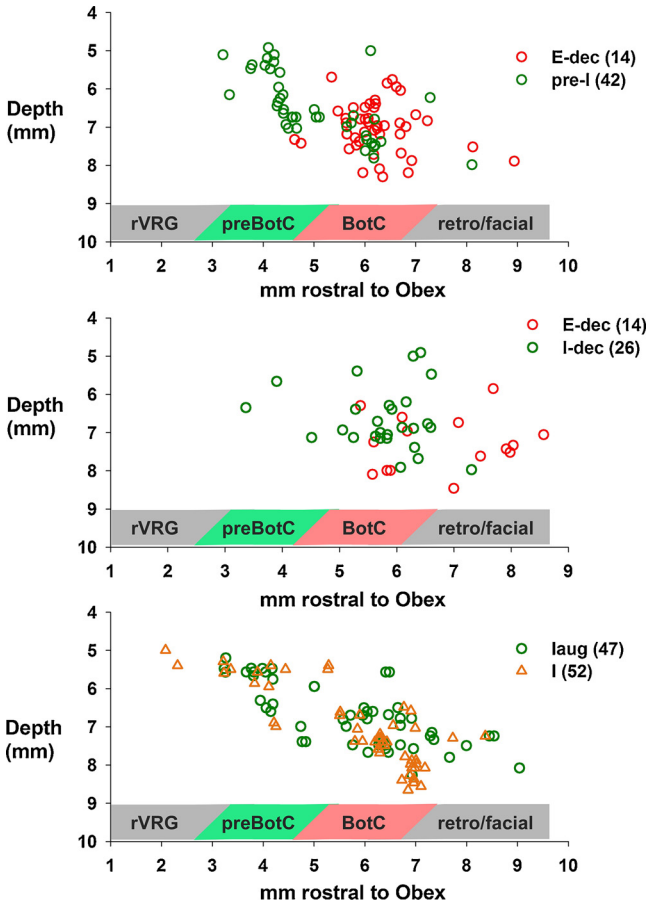

Fig. 11. Anatomical location of neurons receiving Inputs from the pontine subregion based on stereotaxic coordinates relative to the obex, midline and dorsal surface. Plots of depth from the dorsal medullary surface vs. distance rostral to obex. Neuron subtypes and number of neurons are indicated in each plot. The shaded bar below indicates the approximate location within the VRC. See text for details.

bringing them to a threshold level where regenerative recurrent excitation switches them to the full on-state (Butera et al., 1999). Once triggered, the pre-I neurons along with the associated neural network produce a complete inspiratory pattern manifested by the ramp-like PNG pattern (Janczewski et al., 2013; Krolo et al., 2000; Segers et al., 1987). Previously, we have shown that a delayed, short stimulus train was capable of triggering a full eupneic PNG pattern, demonstrating that regenerative elements must be involved in the generation of the phrenic burst in vivo (Zuperku et al., 2017). The present study shows that other subtypes of I-neurons were also excited by the pontine input (e.g., Fig. 10B), which could increase the overall excitability of the inspiratory network. These results provide evidence for one of the major mechanistic components that contribute to controlling the initiation of the I-phase and thus breathing frequency as illustrated in the hypothetical model shown in Fig. 13 (green arrows). This model assumes that the medullary rhythm generation network includes conditional bursting pacemaker neurons of the form modeled by (Butera et al., 1999), which increase their burst rate when excitation is increased (e.g., Fig. 1 in (Del Negro et al., 2009) and act as an interconnected group pacemaker system (Feldman and Del Negro, 2006). These pacemaker neurons, shown as pre-I neurons (Funk and Greer, 2013) or I-driver neurons, supply phasic excitation to the pattern generating circuitry, depicted by reciprocal inhibitory interactions among the I and E neurons in the preBötC/BötC region (Fig. 13). Since both AMPA microinjections and electrical stimuli increase PB subregion neuronal activity and result in shortening of TE, and decreases in PB subregion neuronal activity by inhibitory agents prolong TE, we conclude that this pontine input is excitatory in nature and more specifically increases excitation to the group pacemaker neurons, leading to an earlier onset of the I phase (red input, Fig. 13).

4.2. Inhibition of medullary E-neurons in the Bötzinger region

A second mechanism for advancing the onset of the I-phase is suggested by the finding that many of the E-neurons in the BötC region were strongly inhibited by the inputs from the pontine subregion (e.g., Fig. 5 and 10 A, Area). It is well known that E-neurons synaptically inhibit I-neurons and the principle of reciprocal inhibition has formed the foundation of many network models of the generation and control of respiratory phase durations and neuronal discharge patterns

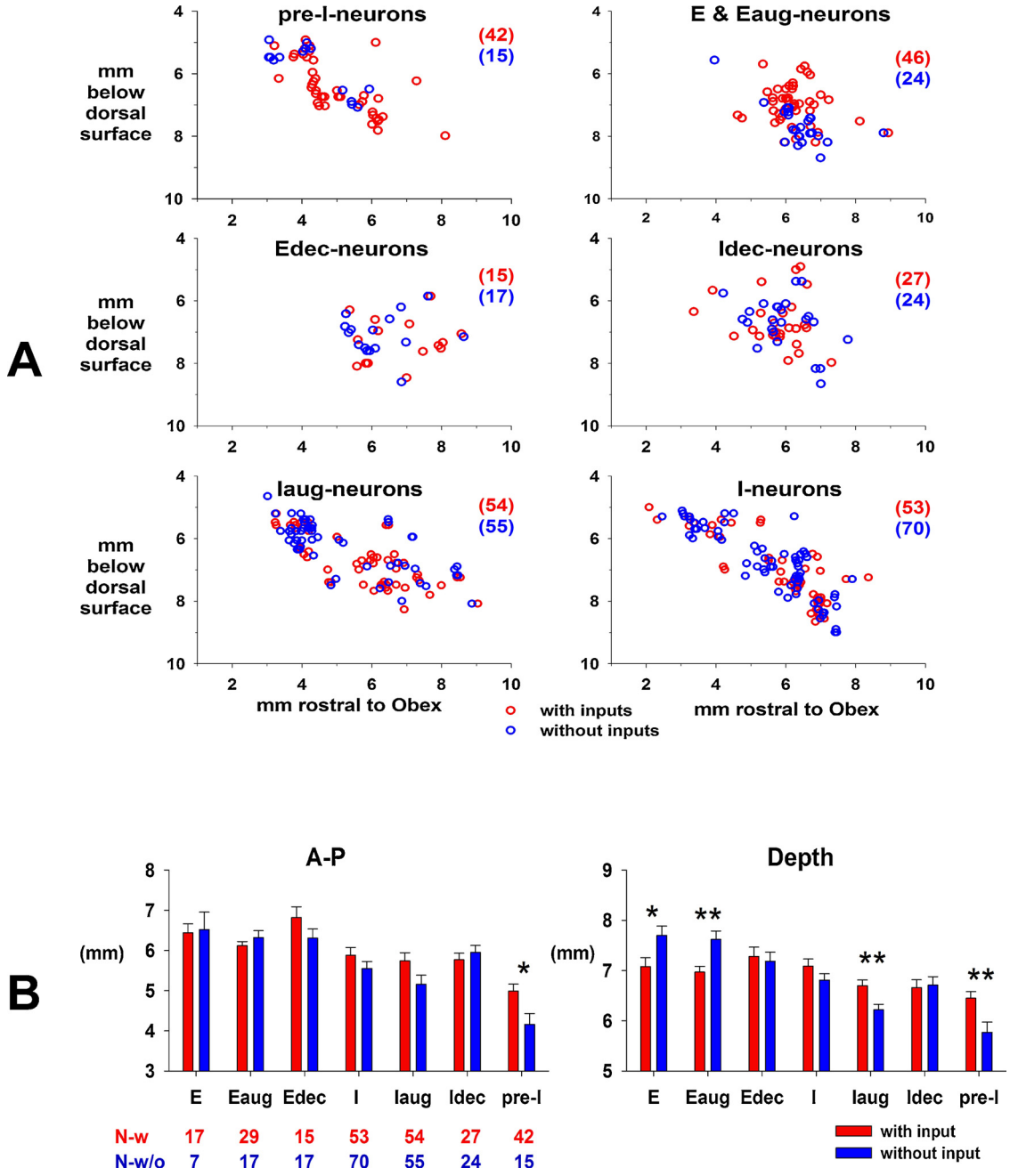

Fig. 12. A) Anatomical location of each neuron subtype that receives a synaptic input from the PB subregion (red) superimposed on those without a detectable input from the PB subregion (blue). E- and E-aug neurons are pooled. B) Comparison of the location rostral to obex caudal and the depth locations of neurons with (red) and without (blue) synaptic inputs. Number of neurons for each subtype below the left bar graph. Statistical comparisons show that pre-I neurons receiving inputs were rostral (left graph) and deeper (right graph) than those without inputs. Differences in depth were seen for I-aug, E-aug and E neurons. See text for details.

(Dutschmann and Dick, 2012; Richter and Smith, 2014; Rybak et al., 2008; Smith et al., 2007). Thus the pontine subregion inhibition of E-neurons would aid to disinhibit I-neurons in the preBötC region (thick red line, Fig. 13) allowing excitatory inputs to the I-neurons to be more effective in switching on the I-phase. More specifically, most of these current network models show an inhibitory input to the pre-I neuron population from the E-dec neurons. The synergistic effects of the nearly simultaneous removal of inhibition and an increase in excitation of the pre-I neurons by the pontine subregion would lead to an efficient robust mechanism to switch on the I-phase. The data from the current study that shows excitation of pre-I neurons and inhibition of E-dec neurons (Fig. 9) is consistent with this possible mechanism.

Since the major focus of this study is on the control of phase-timing, our hypothetical model includes the reflex control of TI and TE by the slowly adapting PSRs mediated via the nucleus of the solitary tract. Bidirectional interactions are shown with the medullary rhythmogenic region and the pons, since interactions between the pons and the medulla have been described (Dutschmann and Dick, 2012).

4.3. Limitations of the methodology

Qualitatively similar results in phase-timing were seen comparing electrical activation of the pontine subregion with local AMPA microinjections (Zuperku et al., 2017). It is known that AMPA directly excites neurons by activation of glutamatergic receptors leading to depolarization, while electrical stimulation potentially stimulates neurons and

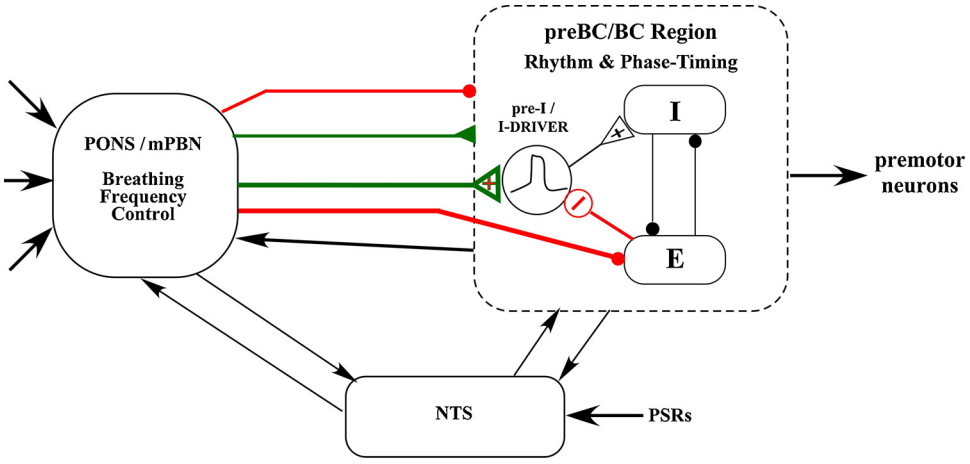

Fig. 13. Diagram of a hypothetical model for terminating the E-phase and advancing the I-phase. The pontine subregion in the medial PB nucleus region (mPBN) sends excitatory inputs (green) to the pre-I as well as other I-neurons to increase pre-I activity and I-phase network excitability to a level that triggers the regenerative properties of the pre-I pacemaker-like neurons and simultaneously strongly inhibits (red) the Bötzinger E-neurons. In addition, Inhibition of the E-neurons results in a possible disinhibition of pre-I neurons (Rybak et al., 2008), which contributes to the increase in pre-I activity and earlier onset of the E-to-I phase switch. These proposed mechanisms shorten the E-phase and switch on the I-phase. The top two inputs (thin lines) indicate general excitatory and inhibitory inputs to the pre-BötC/BötC region. Second order neurons relaying pulmonary stretch receptor activity interact bidirectional with the medullary rhythm/pattern generator and the pontine subregion to control phase timing associated with degree of lung inflation.

fibers of passage. However, since the locations and TE responses were qualitatively similar for both types of stimuli, we hypothesize that both stimuli were acting on the same neurons. We adjusted the stimulus current strength to be about 20–40% greater than the threshold for observing a noticeable but weak response. Since a concentric bipolar electrode with a separation between the inner and outer electrode of ~175 μm was used in conjunction with an isolated constant current stimulator and currents typically 100 μA with a duration of 100 μsec, the current density was very localized. This is supported by the fact that when the stimulus electrode was positioned > 1-mm from the optimal location, a tachypneic response was not observed. Another supporting observation for a localized effect was the small narrow stimulus artifact that is generated when recording unit activity from the medullary VRC neurons that are located 8- to 14-mm from the pontine stimulus site.

Isocapnic hyperoxia was used during these experiments to maintain a constant level of CO2 mediated excitation to the respiratory network during the data recording sessions. Hyperoxia (FIO2 < 0.6) was used to ensure adequate oxygenation of the preparation with extensive surgery and blunt the input from the carotid body chemoreceptors to minimize potential confounding effects. We assume these baseline conditions will have minimum qualitative effects on the synaptic connection data, while it may be possible that the strength of the connections may differ from those during normocapnic/normoxic conditions.

4.4. Possible activation of other functional pathways

It is possible that stimulation in this PB subregion induced neural activity in pathways that are involved with other functions, for example, recruitment of pacemaker-like neurons that do not normally control breathing but are more involved in the regulation of phase-timing for a non-breathing behavior. Our previous study showed that the PB subregion stimuli shortened the E phase without any change in the profile of the following PNG pattern, which appeared no different from those that occurred spontaneously (Zuperku et al., 2017). In contrast, in models of fictive cough large augmentations in PNG amplitude with increased TI are observed when cough is induced (Segers et al., 2012; Shannon et al., 2000). In the current study, the activity of the E-neurons was strongly inhibited by the pontine input rather than augmented as would be expected with active expiratory effort during cough. It might be expected that other types of non-breathing behavior may also be manifested by altered I patterns. In contrast, our present data suggest that electrically induced activity in the PB subregion activated medullary pacemaker-like neurons involved in the generation of the eupneic inspiratory burst pattern TE as manifested by an unchanged PNG pattern following a stimulus in the previous cycle, which shortened TE.

4.5. Nature of electrically-induced activity in the pontine subregion

Electrically evoked tachypneic responses were more robust than those induced by AMPA microinjections (Zuperku et al., 2017). This is most likely due to synchronous activation of neurons that would lead to more efficient spatial summation in the target region. This method of determining synaptic inputs, which showed that ~54% of the recorded VRC neurons received a synaptic input from the pontine subregion, appears to be much less labor intensive in terms of correlation analysis than the more discriminating method of spike-to-spike correlations. For example, Segers et al. (Segers et al., 2008) analyzed the correlogram features of 3218 pairs composed of a PRG and a VRC neuron and found significant offset features for 37 of the 145 (~26%) recorded PRG neurons in cats. In addition, a more recent study reported evidence for a "multi-synaptic" pathway from the pons to the VRC via intermediary brainstem midline raphe´ neurons (Nuding et al., 2009). For example, of the 3067 PRG–raphe´ neuron pairs, significant offset peaks and troughs were detected for 31 of the 145 (21.4%) PRG neurons, while for the raphe´-VRC (6755 pairs), 45 of 285 (15.8%) raphe´ neurons evaluated had significant correlations. Overall, in all recordings, 45 PRG-to-raphe´-to-VRC functional connectivity chains were detected (Nuding et al., 2009). Using antidromic stimulation in rats, Ezure and Tanaka (Ezure and Tanaka, 2006) found ~58% of the respiratory-related neurons in the KF region projected to the medulla with ~30% of those having axons in the ventrolateral NTS and hypoglossal motor regions and ~58% of those with axons in the ventrolateral medulla.

In the current study, the magnitude and duration in the changes in the probability of firing following a stimulus pulse (e.g., PSTHs in Figs. 4, 6 and 8) are far larger than the spike-train cross correlations observed between synaptically coupled neurons (e.g., Figs. 3 and 4 in (Segers et al., 1987). The wider durations of the significant deviations may be due to the summation of synaptic inputs produced by the arrival of action potentials with different conduction velocities that converge (spatial summation) on the recorded neuron. The Area under the deviation would reflect the effects of this efficient form of summation produced by a volley of inputs. Also, the number of deviations with distinct latencies in the PSTHs (e.g., Fig. 8) manifests the effect of inputs with different conduction velocities. Since a pathway from some PRG neurons to medullary VRC neurons involves midline raphe (Nuding et al., 2009), it is possible that a polysynaptic relay pathway may mediate some of the longer latency, broader PSTH deviations.

The canine pontine subregion contains a variety of neuron subtypes

including phasic I-, E-, phase-spanning and non-respiratory modulated tonic neurons (Zuperku et al., 2015b). The relatively weak electrical stimuli within the subregion likely activate several of the neuron subtypes, and thus a synaptic input to a medullary neuron cannot be attributed to a particular PRG neuron subtype using this method. Since the PSTHs for many of the medullary neurons show multiple positive and/or negative significant deviations, this suggests that the medullary neurons receive inputs from one or more PRG subtype neurons.

Typically the PSTH deviation durations were greater than 1-msec and more often in the 2–3 ms range (Fig. 9B, lower). These durations are much longer that those that would result from antidromic activation of the recorded neuron with a fiber projection to the pontine subregion. The latencies of antidromically-activated neurons are very consistent and have very little time-jitter resulting in very narrow positive PSTH deviations (e.g., (Ezure and Tanaka, 2006; Ezure et al., 2003; Krolo et al., 2005). Also, the negative deviations seen in many of the neurons are not the result of antidromic activation of the recorded neurons. Thus, we feel confident that the significant deviations in the PSTHs are the result of synaptic inputs to the medullary neurons.

4.6. Anatomical location of respiratory neuron subtypes

In each experiment, the caudal to rostral tilt angle of the medulla was measured and used to correct the stereotaxic coordinates, which were referenced with respect to the obex, midline, and dorsal surface. This correction has a significant effect on the calculated electrode location. For example at a depth of 7.0-mm, the electrode tip location is actually 0.34-mm and 2.3-mm rostral to the dorsal surface insertion point for tilt angles of 2.8 and 19.0 degrees (5^{th} and 95^{th} percentile values), respectively. The corresponding depths are ~7.0 and 6.62-mm, respectively.

The estimated extent of the preBötC was based on the location of the pre-I neurons (green shaded bar segment, Fig. 11) and is consistent with a previous study of neurons in the preBötC region of dogs (Fig. 7, (Krolo et al., 2005). A study of the subtypes of respiratory neurons in the preBötC region of cats showed that pre-I neurons were intermingled in a dense cluster with many different subtypes of I- and E-neurons in a zone that extended from 3.0 to 3.5-mm rostral to obex (Schwarzacher et al., 1995). These findings were taken as a means to define the preBötC region. That study also defined the BötC by the high density of E-aug neurons adjacent to the preBötC. This finding is also consistent with those of the current study that showed the E- and E-aug neurons located rostral to the pre-I neurons ($p < 0.001$). An interesting finding was that ~2/3rds of the E- and E-aug neurons received an input from the pontine subregion and were dorsal to the $1/3^{rd}$ without inputs (Fig. 12). About $3/4^{th}$ of the pre-I neurons received a pontine input and were located more rostral and ventral to the $1/4^{th}$ without a subregion input (Fig. 12). For all neuron subtypes, 53.6% received at least one pontine subregion input. Such a rich innervation of the medullary neurons from this relatively small pontine subregion is remarkable and suggests the importance of its role in the control of breathing.

4.7. Functional role of the pneumotaxic center

Much of the literature suggests that one of the main roles of the pontine pneumotaxic center is the regulation of the inspiratory-expiratory (IE) phase transition, also referred to as the inspiratory off-switch (IOS, e.g., (Dutschmann and Dick, 2012). The disruption of this rostrolateral pontine region by either electrolytic lesion (Feldman and Gautier, 1976; Oku et al., 1992; St John et al., 1971) or microinjection of drugs (Dutschmann and Herbert, 2006; Ling et al., 1994) that inhibit or block neuronal activity have shown that an apneustic pattern (maintained phrenic discharge following the initial period of augmenting discharge) is observed when pulmonary afferent input is reduced, for example by preventing lung inflation. In our current and a previous study (Zuperku et al., 2017), activation or inhibition (Zuperku et al., 2015a) of neurons in a subregion of the medial PB region in dogs affected the E-to-I phase transition or inspiratory on-switch. In comparing the histological sections showing the pneumotaxic region in cats (Feldman and Gautier, 1976; Oku et al., 1992; St John et al., 1971) with the subregion in dogs (Zuperku et al., 2017), the locations appear to overlap suggesting that the differing functions may be due to species differences. Alternatively, the different functions may be due to anatomically different locations. (Cohen, 1971) using localized electrical stimulation via a small bipolar electrode in and near the PB region in decerebrate cats was able to show two distinct regions with opposing responses: (a) at dorsolateral points, inspiratory-facilitatory effects (increase of phrenic discharge, shortening of the expiratory phase); (b) at ventrolateral points, expiratory-facilitatory effects (decrease of phrenic discharge, shortening of the inspiratory phase, lengthening of the expiratory phase). Similar findings were observed by Bertrand and Hugelin (Bertrand and Hugelin, 1971) where they found that single and double shock excitation of the dorsomedial part of the NPBM more frequently triggered inspiration, whereas excitation of its lateral part in the lemniscus lateralis region more often provoked an immediate cessation of the phrenic burst.

Since the size of the lesions and size of the microinjections appear to overlap the more ventral region in the cats, it is likely that this inspiratory-inhibitory/expiratory-facilitatory region was disrupted. Since electrical stimulation of this region that is confined to the I-phase shortens TI and terminates the I-phase, disruption of its function would lead to the loss of an excitatory input to the IOS, leading to apneusis in the absence of PSR input. Furthermore in support of this alternative explanation, Hurle (Hurle et al., 1985) observed that opioids applied to the dorsal surface of the rostrolateral pons in anesthetized and decerebrate cats resulted in a decrease in breathing frequency with little change in tidal volume. These results are consistent with those observed in dogs (Prkic et al., 2012) and rabbits (Miller et al., 2017), where localized microinjections of DAMGO in the PB region resulted in bradypnea and apnea without changes in peak phrenic activity. The subregion of the current study is within the mapped PB region in which DAMGO induced apnea. Thus, it is likely that the pontine location rather than species difference could explain the differences observed in the control of phase-timing. Since the apneusis pattern is often observed in the cat, but appears less often in the dog (ejz personal observation), a quantitative difference between species may exist. At this time, we have not explored the effects of localized electrical stimulation at more ventral locations for TI shortening-TE lengthening in the canine pons.

4.8. Physiological significance

This PB subregion appears to play a key role in the control of breathing frequency (fB). Excitation of the subregion neurons produces a rapid increase in fB with latencies < 200 ms, while inhibition of these neurons by localized microinjections of opioids and inhibitory drugs produce bradypnea and sustained apnea, reversible with appropriate antagonists. It is remarkable that this subregion can powerfully control TE without altering the magnitude and time course of the ramp-like PNG (Zuperku et al., 2017). A short 100–200 ms pulse-train can terminate the E-phase and trigger the I-phase resulting in a eupneic ramp-like phrenic burst pattern. A highly plausible explanation for this observation is that the I-burst generator must contain neurons with regenerative, pacemaker-like properties, suggesting that preBötC pacemaker-like neurons are fully active during eupneic breathing in vivo. The rapid activation of the medullary inspiratory-generating network appears to be brought about by the dual action of rapid inhibition of E-neurons and rapid excitation of I-neurons, notably the pre-I neurons (Fig. 10A, latencies). Thus, it would appear that these rapid dynamics would allow this pontine subregion to provide a site for integration of sensory afferents involved with coordinating other behaviors related to breathing, such as swallowing, sneezing, and other cranial sensory inputs. For example the trigeminal sensory region is located in close

proximity to this pontine subregion and provides sensory input that mediates the nasotrigeminal reflex that prevents invasion of noxious substances into the upper airways causing apnea in the expiratory phase and plays a key role in the diving response of aquatic mammals, which is induced by face immersion (Dutschmann and Herbert, 1998).

The location of the PB-KF complex is midway between the forebrain and medulla, where it receives numerous descending and ascending projections that mediate and process emotion and pain and associated breathing pattern responses (Jiang et al., 2004). It has been suggested that the PB nuclei may play an important role in integrating respiratory-related afferents with other afferents such as nociceptive, thermosensitive, somatic proprioceptive, and cardiovascular-related afferents (Jiang et al., 2004; Morrison et al., 2008; Potts et al., 2005; Song et al., 2006) and coordination of cardiorespiratory function (Dick et al., 2009). The descending forebrain inputs and efferent connectivity with important sensory relay nuclei in brainstem and spinal cord support the important role of rostral pons in the gating of adaptive breathing during behavior, emotion, and associated homeostasis (Dutschmann and Dick, 2012). In addition, the gain of the Hering-Breuer reflex, which is mediated by slowly-adapting pulmonary stretch receptors and plays a key role in controlling TI and TE, is modulated by the PB-KF complex (Dhingra et al., 2017).

The medial PB subregion may also play a key role in mediating the rapid ventilatory response to exercise as well as the sustained response. At the very onset of exercise, pulmonary ventilation rapidly increases, with a time constant of a few seconds (phase I) before feedback mechanisms become effective, suggesting the involvement of a central command or feed-forward neural mechanism (Forster et al., 2012; Waldrop and Iwamoto, 2006). Central command is viewed as a parallel, simultaneous excitation of neuronal circuits controlling the locomotor and cardiorespiratory systems (Eldridge et al., 1985). Interestingly, in the cat the mesencephalic locomotive region (MLR) (near the cuneiform nucleus; (Garcia-Rill and Skinner, 1987) is located 1–1.5 mm rostral and ~2 mm dorsal from the PB tachypneic subregion. The results of a recent study in lampreys shows that neurons in the respiratory generator network receive direct glutamatergic connections from the MLR and that a subpopulation of MLR neurons plays a key role in the respiratory changes linked to movement (Gariepy et al., 2012). When the mesencephalic locomotive region is electrically stimulated in a decerebrate cat, the rate of locomotion increases as a quasi-linear function of stimulus intensity (Le Ray et al., 2011) analogous to the PB subregion increase in breathing frequency (Zuperku et al., 2017). A recent theoretical-modeling study of the spinal locomotor central pattern generator clearly shows a quasi-linear relationship between breathing frequency and descending tonic excitatory inputs (Ausborn et al., 2018) in agreement with the in vivo results (Zuperku et al., 2017). Thus it is possible that PB subregion participates in the feed-forward command of the isocapneic hyperpneic response induced with exercise. Since during steady-state exercise both breathing frequency and tidal volume significantly increase in proportion to the amount of CO2 excretion (e.g., Fig. 3 in (Forster et al., 2012), the PB subregion may also participate in the feedback mechanism.

This subregion is sensitive to clinical concentrations of opioids, which produce bradypnea and even apnea at higher concentrations (Miller et al., 2017; Prkic et al., 2012). Within the PB-KF nuclei, a multitude of neurotransmitters/modulators and their associated receptors have been identified by in situ hybridization, immunocytochemistry, and neuronal responses to locally applied antagonists. These receptors may serve as potential therapeutic drug targets to counteract respiratory depression produced by opioids and sedatives. Thus, drugs that affect neuronal activity in this PB subregion can have a major impact on breathing rate.

4.9. Conclusion

In conclusion, a subregion within the medial PB complex plays a key role in the control of TE, the switching on of the I-phase, and breathing rate. The rapid activation of the medullary inspiratory-generating network appears to be brought about by the dual action of rapid inhibition of medullary E-neurons and rapid excitation of the medullary I-neurons, including the pre-I neurons, mediated by the medial PB subregion.

Acknowledgments

This work was supported by Merit Review Award 5 I01 BX000721-07 from the Department of Veterans Affairs Biomedical Laboratory Research and Development Program (E.J. Zuperku, PI); the National Institutes of Health Grant 1 R01 GM112960-01 (A.G. Stucke, PI); the Department of Anesthesiology, Medical College of Wisconsin; and the Children's Hospital of Wisconsin.

References

Ausborn, J., Snyder, A.C., Shevtsova, N.A., Rybak, I.A., Rubin, J.E., 2018. State-dependent rhythmogenesis and frequency control in a half-center locomotor CPG. J. Neurophysiol. 119, 96–117.
Bertrand, F., Hugelin, A., 1971. Respiratory synchronizing function of nucleus parabrachialis medialis: pneumotaxic mechanisms. J. Neurophysiol. 34, 189–207.
Butera Jr, R.J., Rinzel, J., Smith, J.C., 1999. Models of respiratory rhythm generation in the pre-Bötzinger complex. I. Bursting pacemaker neurons. J. Neurophysiol. 81, 382–397.
Cohen, M.I., 1971. Switching of the respiratory phases and evoked phrenic responses produced by rostral pontine electrical stimulation. J. Physiol. (London) 217, 133–158.
Del Negro, C.A., Kam, K., Hayes, J.A., Feldman, J.L., 2009. Asymmetric control of inspiratory and expiratory phases by excitability in the respiratory network of neonatal mice in vitro. J. Physiol. 587, 1217–1231.
Dhingra, R.R., Dutschmann, M., Galan, R.F., Dick, T.E., 2017. Kolliker-Fuse nuclei regulate respiratory rhythm variability via a gain-control mechanism. Am. J. Physiol. Regul. Integr. Comp. Physiol. 312, R172–R188.
Dick, T.E., Baekey, D.M., Paton, J.F., Lindsey, B.G., Morris, K.F., 2009. Cardio-respiratory coupling depends on the pons. Respir. Physiol. Neurobiol. 168 (Aug. (1-2)), 76–85.
Dutschmann, M., Dick, T.E., 2012. Pontine mechanisms of respiratory control. Compr. Physiol. 2, 2443–2469.
Dutschmann, M., Herbert, H., 1998. NMDA and GABAA receptors in the rat Kolliker-Fuse area control cardiorespiratory responses evoked by trigeminal ethmoidal nerve stimulation. J. Physiol. 510 (Pt. 3), 793–804.
Dutschmann, M., Herbert, H., 2006. The Kolliker-Fuse nucleus gates the postinspiratory phase of the respiratory cycle to control inspiratory off-switch and upper airway resistance in rat. Eur. J. Neurosci. 24, 1071–1084.
Eldridge, F.L., Millhorn, D.E., Kiley, J.P., 1985. Stimulation by central command of locomotion, respiration and circulation during exercise. Respir. Physiol. 59, 313–337.
Euler, C.V., 1986. Brain stem mechanisms for generation and control of breathing pattern. In: Cherniack, N.S., Widdecombe, J.G. (Eds.), Handbook of Physiology The Respiratory System. Am. Physiol. Soc., Bethesda, MD, pp. 1–67.
Ezure, K., Tanaka, I., 2006. Distribution and medullary projection of respiratory neurons in the dorsolateral pons of the rat. Neuroscience 141, 1011–1023.
Ezure, K., Tanaka, I., Saito, Y., 2003. Brainstem and spinal projections of augmenting expiratory neurons in the rat. Neurosci. Res. 45, 41–51.
Feldman, J.L., Del Negro, C.A., 2006. Looking for inspiration: new perspectives on respiratory rhythm. Nat. Rev. Neurosci. 7, 232–242.
Feldman, J.L., Gautier, H., 1976. Interaction of pulmonary afferents and pneumotaxic center in control of respiratory pattern in cats. J. Neurophysiol. 39, 31–44.
Forster, H.V., Haouzi, P., Dempsey, J.A., 2012. Control of breathing during exercise. Compr. Physiol. 2, 743–777.
Funk, G.D., Greer, J.J., 2013. The rhythmic, transverse medullary slice preparation in respiratory neurobiology: contributions and caveats. Respir. Physiol. Neurobiol. 186, 236–253.
Garcia-Rill, E., Skinner, R.D., 1987. The mesencephalic locomotor region. I. Activation of a medullary projection site. Brain Res. 411, 1–12.
Gariepy, J.F., Missaghi, K., Chevallier, S., Chartre, S., Robert, M., Auclair, F., Lund, J.P., Dubuc, R., 2012. Specific neural substrate linking respiration to locomotion. Proc. Natl. Acad. Sci. U. S. A. 109, E84–92.
Hurle, M.A., Mediavilla, A., Florez, J., 1985. Differential respiratory patterns induced by opioids applied to the ventral medullary and dorsal pontine surfaces of cats. Neuropharmacology 24, 597–606.
Jakovcevic, D., Brandes, I., Hopp, F., Stucke, A., Stuth, E., McCrimmon, D., Zuperku, E., 2005. Defining regions within the canine medullary ventral respiratory column (VRC) involved with phase-timing. FASEB J. A472.
Janczewski, W.A., Tashima, A., Hsu, P., Cui, Y., Feldman, J.L., 2013. Role of inhibition in respiratory pattern generation. J. Neurosci. 33, 5454–5465.
Jiang, M., Alheid, G.F., Calandriello, T., McCrimmon, D.R., 2004. Parabrachial-lateral pontine neurons link nociception and breathing. Respir. Physiol. Neurobiol. 143, 215–233.
Krolo, M., Stuth, E.A., Tonkovic-Capin, M., Hopp, F.A., McCrimmon, D.R., Zuperku, E.J., 2000. Relative magnitude of tonic and phasic synaptic excitation of medullary

inspiratory neurons in dogs. Am. J. Physiol. Regul. Integr. Comp. Physiol. 279, R639–R649.
Krolo, M., Tonkovic-Capin, V., Stucke, A., Stuth, E., Hopp, F., Dean, C., Zuperku, E., 2005. Subtype composition and responses of respiratory neurons in the pre-Botzinger region to pulmonary afferent inputs in dogs. J. Neurophysiol. 93, 2674–2687.
Le Ray, D., Juvin, L., Ryczko, D., Dubuc, Rj, Jean Pierre Gossard, Rj D., Arlette, K., 2011. Supraspinal control of locomotion: the mesencephalic locomotor region. Chapter 4. Progress in Brain Research. Elsevier, pp. 51–70.
Lindsey, B.G., Segers, L.S., Shannon, R., 1987. Concurrent distributed processes and intraphase modulation of interactions among medullary respiratory neurons. Evidence from multi-neuron recordings. Respiratory Muscles and Their Neuromotor Control. Alan R. Liss, Inc., pp. 49–53.
Ling, L., Karius, D.R., Speck, D.F., 1994. Role of N-methyl-D-aspartate receptors in the pontine pneumotaxic mechanism in the cat. J. Appl. Physiol. 76 (3), 1138–1143.
Miller, J.R., Zuperku, E.J., Stuth, E.A.E., Banerjee, A., Hopp, F.A., Stucke, A.G., 2017. A subregion of the parabrachial nucleus partially mediates respiratory rate depression from intravenous remifentanil in young and adult rabbits. Anesthesiology 127 (Sep. (3)), 502–514.
Morrison, S.F., Nakamura, K., Madden, C.J., Morrison, S.F., Nakamura, K., Madden, C.J., 2008. Central control of thermogenesis in mammals. Exp. Physiol. 93, 773–797.
Nuding, S.C., Segers, L.S., Baekey, D.M., Dick, T.E., Solomon, I.C., Shannon, R., Morris, K.F., Lindsey, B.G., 2009. Pontine-ventral respiratory column interactions through raphe circuits detected using multi-array spike train recordings. J. Neurophysiol. 101, 2943–2960.
Oku, Y., Tanaka, I., Ezure, K., 1992. Possible inspiratory off-switch neurones in the ventrolateral medulla of the cat. Neuroreport 3, 933–936.
Potts, J.T., Rybak, I.A., Paton, J.F.R., 2005. Respiratory rhythm entrainment by somatic afferent stimulation. J. Neurosci. 25, 1965–1978.
Prkic, I., Mustapic, S., Radocaj, T., Stucke, A.G., Stuth, E.A., Hopp, F.A., Dean, C., Zuperku, E.J., 2012. Pontine mu-opioid receptors mediate bradypnea caused by intravenous remifentanil infusions at clinically relevant concentrations in dogs. J. Neurophysiol. 108, 2430–2441.
Richter, D.W., Smith, J.C., 2014. Respiratory rhythm generation in vivo. Physiology (Bethesda) 29, 58–71.
Rybak, I.A., O'Connor, R., Ross, A., Shevtsova, N.A., Nuding, S.C., Segers, L.S., Shannon, R., Dick, T.E., Dunin-Barkowski, W.L., Orem, J.M., Solomon, I.C., Morris, K.F., Lindsey, B.G., 2008. Reconfiguration of the pontomedullary respiratory network: a computational modeling study with coordinated in vivo experiments. J. Neurophysiol. 100, 1770–1799.
Schwarzacher, S.W., Smith, J.C., Richter, D.W., 1995. Pre-Bötzinger complex in the cat. J. Neurophysiol. 73, 1452–1461.
Segers, L.S., Shannon, R., Saporta, S., Lindsey, B.G., 1987. Functional associations among simultaneously monitored lateral medullary respiratory neurons in the cat: I. Evidence for excitatory and inhibitory actions of inspiratory neurons. J. Neurophysiol. 57 (4), 1078–1100.
Segers, L.S., Nuding, S.C., Dick, T.E., Shannon, R., Baekey, D.M., Solomon, I.C., Morris, K.F., Lindsey, B.G., 2008. Functional connectivity in the pontomedullary respiratory network. J. Neurophysiol. 100, 1749–1769.
Segers, L.S., Nuding, S.C., Vovk, A., Pitts, T., Baekey, D.M., O'Connor, R., Morris, K.F., Lindsey, B.G., Shannon, R., Bolser, D.C., 2012. Discharge identity of medullary inspiratory neurons is altered during repetitive fictive cough. Front. Physiol. 3, 223.
Shannon, R., Baekey, D.M., Morris, K.F., Li, Z., Lindsey, B.G., 2000. Functional connectivity among ventrolateral medullary respiratory neurones and responses during fictive cough in the cat. J. Physiol. 525, 207–224.
Smith, J.C., Abdala, A.P., Koizumi, H., Rybak, I.A., Paton, J.F., 2007. Spatial and functional architecture of the mammalian brain stem respiratory network: a hierarchy of three oscillatory mechanisms. J. Neurophysiol. 98, 3370–3387.
Song, G., Yu, Y., Poon, C.S., 2006. Cytoarchitecture of pneumotaxic integration of respiratory and nonrespiratory information in the rat. J. Neurosci. 26, 300–310.
St John, W.M., Glasser, R.L., King, R.A., 1971. Apneustic breathing after vagotomy in cats with chronic pneumotaxic center lesions. Respir. Physiol. 12, 239–250.
St-John, W.M., Paton, J.F.R., 2003. Defining eupnea. Respir. Physiol. Neurobiol. 139, 97–103.
Tonkovic-Capin, M., Krolo, M., Stuth, E.A.E., Hopp, F.A., Zuperku, E.J., 1998. Improved method of canine decerebration. J. Appl. Physiol. 85, 747–750.
Waldrop, T.G., Iwamoto, G.A., 2006. Point: supraspinal locomotor centers do contribute significantly to the hyperpnea of dynamic exercise. J. Appl. Physiol. (1985) 100, 1077–1079.
Zuperku, E., Prkic, I., Stucke, A., Miller, J., Hopp, F., Stuth, E., 2015a. Neurons in the pontine medial parabrachial (PB) region play a key role in the control of breathing frequency. FASEB J. 29.
Zuperku, E.J., Prkic, I., Stucke, A.G., Miller, J.R., Hopp, F.A., Stuth, E.A., 2015b. Automatic classification of canine PRG neuronal discharge patterns using K-means clustering. Respir. Physiol. Neurobiol. 207, 28–39.
Zuperku, E.J., Stucke, A.G., Hopp, F.A., Stuth, E.A., 2017. Characteristics of breathing rate control mediated by a subregion within the pontine parabrachial complex. J. Neurophysiol. 117, 1030–1042.